sustainability

MDPI

Article

Influence of the Primary Key Stratum on Surface Subsidence during Longwall Mining

Kang Wang [1], Jiazhen Li [1,*] and Zhupeng Jin [2]

[1] College of Mining Engineering, Liaoning Technical University, Fuxin 123000, China
[2] School of Mining Engineering, Heilongjiang University of Science and Technology, Harbin 150027, China
* Correspondence: l.jz2000@163.com

Abstract: The surface subsidence caused by mining influences the mine environment and construction safety. In this paper, strata movement and surface subsidence were combined. Based on elasticity and Winkler theory, a prediction method of surface subsidence was established with the primary key stratum as the research object. Using the Tingnan Coal Mine as an example, the mining subsidence of the second panel was predicted. Comparing the predicted results with the measured results, the causes of errors were analyzed and the field of application of the model was clarified. Besides, the geological and mining factors affecting surface subsidence were also analyzed. The results show that the mining subsidence is the surface manifestation of the strata movement. Surface subsidence is affected by the mining area, load, and flexural rigidity of the primary key stratum, foundation modulus of the goaf, and the rock mass. The research results have significance for the planning of the coal resources and the prevention of geological disasters.

Keywords: surface subsidence; key stratum theory; Winkler foundation; finite difference method; elasticity

Citation: Wang, K.; Li, J.; Jin, Z. Influence of the Primary Key Stratum on Surface Subsidence during Longwall Mining. *Sustainability* **2022**, *14*, 15027. https://doi.org/10.3390/su142215027

Academic Editors: Jianhang Chen, Danqi Li, Ping Chang and Saisai Wu

Received: 29 September 2022
Accepted: 2 November 2022
Published: 14 November 2022

1. Introduction

Coal mining inevitably leads to strata movement and surface subsidence. Unlike underground accidents, surface subsidence involves the general public. It is a direct threat to the ecological environment and construction safety [1–8].

The surface subsidence caused by mining is mainly studied using the influence function method, mechanical method, similar materials experiment, and numerical simulation method. The similar material experiment is conducive to understand the subsidence but limited by the equipment size; the plane strain problem is mainly studied [9,10]. The finite difference method (FDM) cannot simulate the complex process from continuous deformation to discontinuous fracture [11–13]. The discrete element method (DEM) is limited by computational costs [14–16]. The influence function method is widely used in many countries because of its convenience [17–22]. Mining subsidence is the surface manifestation of strata movement, closely related to the lithology and occurrence characteristics of overburden [23–25]. However, the influence function method cannot explain the mechanical mechanism of the strata movement [26,27]. It characterizes the overburden characteristics through limited predicted parameters and requires reliable monitoring data; otherwise, it can easily cause errors [28–30].

Some scholars try to reveal the surface subsidence process through the mechanical mechanism of strata movements. According to the displacement curve of the voussoir beam, the subsidence prediction model of a fractured rock beam forming a stable structure is established [31]. According to the elastic foundation theory [32,33], visco-elastic theory [34], the curved subsidence prediction model of the rock beam is established. According to the elastic thin plate theory [35], the subsidence prediction model under the geological conditions of thick alluvium is established. The beam theory can only establish an overburden profile model. The elastic thin plate model with fixed support is inconsistent with the occurrence characteristics of the overburden [36,37].

Combined with the occurrence characteristics and movement law of mining-induced overburden, this paper focuses on establishing a full-size mechanical model of strata movement. Based on the elasticity and Winkler theory, the research subject proposes a surface subsidence prediction method with the primary key stratum in the continuous deformation zone. The method is applied to a real example: Tingnan Coal Mine, located in the Binchang coalfield, Shanxi Province, China. The research results have important practical significance to resource planning, coal mining design, protection of surface construction, and the prevention of geological disasters.

2. Prediction Method of Surface Subsidence

2.1. Movement Characteristics of Mining-Induced Overburden

It is crucial to determine the characteristics of strata movement to underground work and subsidence prediction. The strata are usually composed of layered sedimentary rocks of varying thicknesses, strengths, and stiffnesses. The bond between layers is weak [38]. Due to the specialty of sedimentary rock, the mining-induced overburden will present different displacements and subsidence velocities. With the increase in roof span, the immediate roof is separated first. It gradually interpenetrates and collapses, forming irregular blocks to fill the goaf [36,37]. With the increase in the mining excavation area, the fracture region of overburden expands upward. The fracture of the main roof will form a voussoir beam structure if it does not slip and rotate instability [39].

With the increase in fracture region, the height of residual space decreases due to the fragmentation and expansion of the fracture strata. The fracture strata are full of mining space. According to the continuity of strata, Syd S. Peng divided the longwall mining overburden into caved, fractured, and continuous deformation zones [40], as shown in Figure 1. The overburden movement caused by mining is finally transmitted to the surface. The elastic deflection of the continuous deformation zone far away from the mining area causes the surface movement basin.

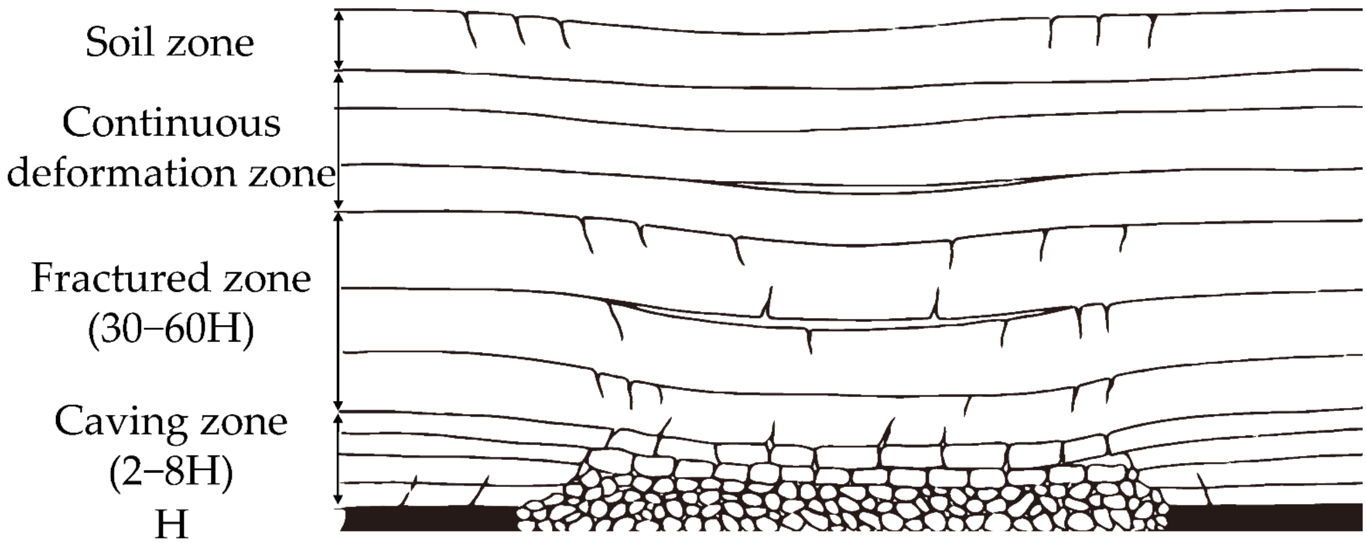

Figure 1. The zoning of the overburden above goaf.

2.2. Key Stratum Theory

The academician Qian pointed out that, as the primary bearing structure, the hard and thick stratum plays a controlling role in the movement and deformation of mining-induced overburden, which is called the key stratum [41]. Other weak strata only have a loading effect and the key stratum bears their loads. The overburden can be divided into many strata groups by the key stratum. The key stratum moves synchronously with the strata it controls, but the key stratum groups move asynchronously. The discriminant method of key stratum is as follows:

Firstly, the stiffness of the stratum is discriminated against to find out the possible location of the key stratum. Because the load of the key stratum does not need the lower stratum to bear, the deflection of the key stratum is less than that of the lower stratum. The calculation model of the key stratum's load is shown in Figure 2. It is assumed that there are m strata in the overburden and the No. 1 stratum is the first hard and thick stratum, which is controlled to the nth stratum to form a composite beam structure. If the No. $n + 1$ stratum is the second hard and thick stratum, it must satisfy:

$$q_1|_{n+1} < q_1|_n \tag{1}$$

where $q_1\,|\,_n$, and $q_1\,|\,_{n+1}$ are loads of the first hard and thick stratum calculated to the nth stratum and the n+1 stratum. According to the theory of composite beams, the formula for calculating $q_1\,|\,_n$ is:

$$q_1|_n = \frac{E_1 {h_1}^3 \sum_{i=1}^{n} \gamma_i h_i}{\sum_{i=1}^{n} E_i {h_i}^3} \tag{2}$$

where $E_1, E_2, \ldots, E_n; h_1, h_2, \ldots, h_n; \gamma_1, \gamma_2, \ldots, \gamma_n$ are the elastic modulus, thickness, and volume force of the hard and thick stratum and controlled strata. Each stratum must be distinguished from bottom to top until all the hard thick stratum that may become the key stratum are finally found.

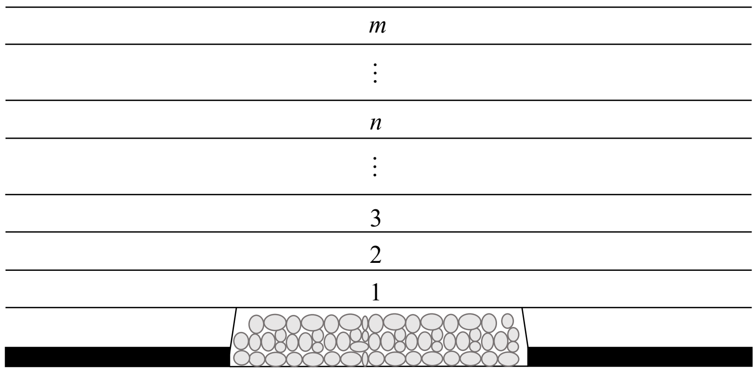

Figure 2. The calculation model of the key stratum's load.

Then, the strength of the possible key strata are discriminated. The fracture distance of the lower hard and thick stratum is less than that of the upper hard and thick stratum. The discriminant method is:

$$l_j < l_{j+1}\ (j = 1, 2, \cdots, k) \tag{3}$$

where l_j and l_{j+1} are the fracture distance of the jth and j+1st of the hard and thick stratum; k is the total number of hard and thick strata. The l_j and l_{j+1} can be estimated according to the theory of the fixed beam.

$$l_j = h_j \sqrt{2R_t / q_j} \tag{4}$$

where q_j and R_t are the load and tensile strength of the jth hard and thick stratum.

Distinguish each stratum from bottom to top until all the key strata are finally found. The key stratum that controls the local strata is called the inferior key stratum (IKS). The key stratum that controls all the strata until the surface is called the primary key stratum (PKS). The key stratum affects the mine pressure behavior and controls the surface movement [42].

2.3. Construction of Prediction Model

Han et al. monitored the relative movement of the PKS and the surface in the process of longwall mining [31]. The results show that the deformation value of the PKS is approximately equal to the surface subsidence value when the mining-induced strata have a continuous deformation zone. Therefore, according to the key stratum theory, the movement of the PKS can be approximated as surface subsidence.

The research scope is limited to the horizontal layered PKS in the continuous deformation zone. According to the occurrence characteristics of overburden, the full-size structural mechanics model of PKS is established. Assuming that the PKS is a clamped plate [43], which is rectangular and bears a uniform load. Based on these assumptions, the following restrictions are imposed [36,37,44,45]:

(1) The middle plane of the plate coincides with the centerline of PKS;
(2) The length of the PKS exceeds 5–8 times its thickness;
(3) The deflection of the PKS is far less than its thickness;
(4) The PKS is elastic, homogeneous, and isotropic;
(5) The complete rock mass and fractured rock mass below the PKS satisfy the Winkler elastic foundation theory;
(6) The lateral pressure has almost no influence on subsidence [46], so the mechanical model ignores the horizontal stress. The full-size structural mechanics model of the PKS is shown in Figure 3, α is the fracture angle of the rock strata. As shown in the top view of the PKS, the A1B1C1D1 area is the goaf-supported zone and the ABCD area around the goaf-supported zone is the rock mass-supported zone. As shown in the section of the PKS, the PKS is clamped by relatively weak rock strata. The elastic foundation supports the rock mass supported-zone and goaf supported-zone [47]. The load of the goaf supported zone is q, which is the sum of self-weight and controlled weak rock strata load.

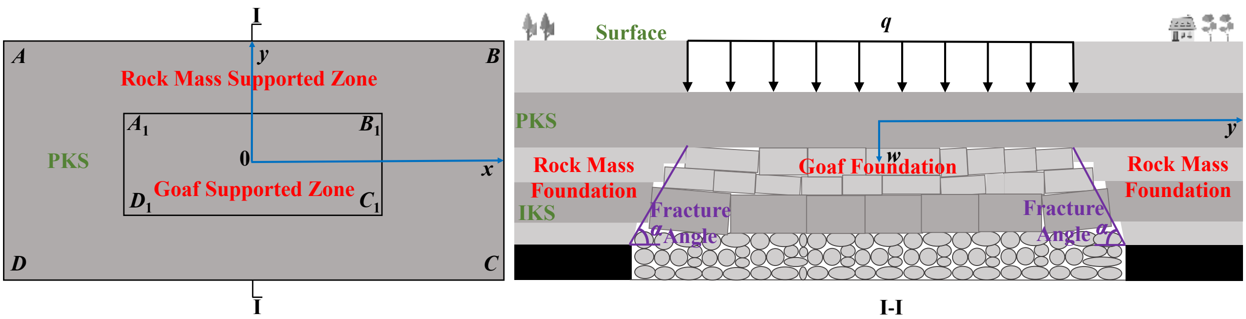

Figure 3. The mechanics model of the PKS.

The basic differential equations of PKS in the goaf supported zone and rock mass supported zone are as follows:

$$\frac{\partial^4 w_g}{\partial x^4} + 2\frac{\partial^4 w_g}{\partial x^2 \partial y^2} + \frac{\partial^4 w_g}{\partial y^4} + \frac{k_g w_g}{D} = \frac{q}{D} \tag{5}$$

$$\frac{\partial^4 w_r}{\partial x^4} + 2\frac{\partial^4 w_r}{\partial x^2 \partial y^2} + \frac{\partial^4 w_r}{\partial y^4} + \frac{k_r w_r}{D} = 0 \tag{6}$$

where w_g and w_r are the deflection functions of the goaf supported zone and rock mass supported zone; D is the flexural rigidity of PKS; $D = Eh^3/12(1-\mu^2)$; q is calculated by Formula (2); k_g and k_r are the foundation modulus of the fracture rock strata in goaf and complete rock mass around the goaf.

The differential equations of the fixed boundary around the rock mass supported zone are as follows:

$$\begin{cases} AB\ \{w_2 = 0; \partial w_2/\partial y = 0 \\ CD\ \{w_2 = 0; \partial w_2/\partial y = 0 \\ AD\ \{w_2 = 0; \partial w_2/\partial x = 0 \\ BC\ \{w_2 = 0; \partial w_2/\partial x = 0 \end{cases} \tag{7}$$

Combined with the boundary conditions, the deflection value obtained through the basic differential equations of the two zones is the subsidence value of the PKS.

2.4. Finite Difference Method

The differential equations are solved by the finite difference method. As shown in Figure 4, the middle plane of the PKS is drawn into difference grids and nodes, δ is the length of the grid spacing. The finite difference method uses difference equations to express the differential equations [36,37,48,49].

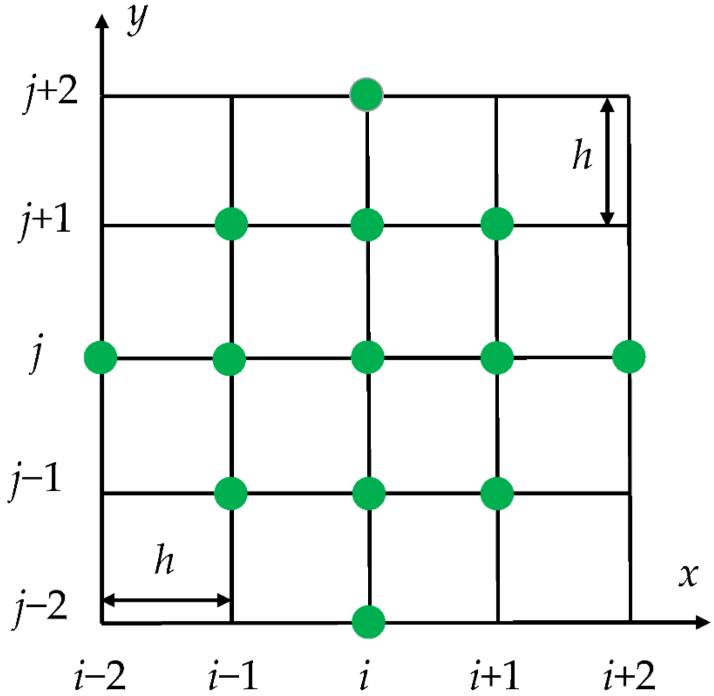

Figure 4. The differential grids and nodes.

The basic difference equations of PKS in the goaf supported zone and rock mass supported zone are as follows:

$$\begin{gathered}\frac{q\delta^4}{D} = \left(20 + \frac{k_g\delta^4}{D}\right)w_g(i,j) - 8\begin{bmatrix} w_g(i+1,j) + w_g(i,j+1) \\ +w_g(i-1,j) + w_g(i,j-1) \end{bmatrix} \\ +2\begin{bmatrix} w_g(i+1,j-1) + w_g(i+1,j+1) \\ +w_g(i-1,j+1) + w_g(i-1,j-1) \end{bmatrix} + \begin{bmatrix} w_g(i+2,j) + w_g(i,j+2) \\ +w_g(i-2,j) + w_g(i,j-2) \end{bmatrix}\end{gathered} \tag{8}$$

$$\begin{gathered}0 = \left(20 + \frac{k_r\delta^4}{D}\right)w_r(i,j) - 8\begin{bmatrix} w_r(i+1,j) + w_r(i,j+1) \\ +w_r(i-1,j) + w_r(i,j-1) \end{bmatrix} \\ +2\begin{bmatrix} w_r(i+1,j-1) + w_r(i+1,j+1) \\ +w_r(i-1,j+1) + w_r(i-1,j-1) \end{bmatrix} + \begin{bmatrix} w_r(i+2,j) + w_r(i,j+2) \\ +w_r(i-2,j) + w_r(i,j-2) \end{bmatrix}\end{gathered} \tag{9}$$

The difference equations of the fixed boundary around the rock mass supported zone are as follows:

$$\begin{cases} AD\ \{w_r(i,j) = 0; w_r(i-1,j) = 3w_r(i+1,j) - w_r(i+2,j)/2 \\ BC\ \{w_r(i,j) = 0; w_r(i+1,j) = 3w_r(i-1,j) - w_r(i-2,j)/2 \\ AB\ \{w_r(i,j) = 0; w_r(i,j+1) = 3w_r(i,j-1) - w_r(i,j-2)/2 \\ CD\ \{w_r(i,j) = 0; w_r(i,j-1) = 3w_r(i,j+1) - w_r(i,j+2)/2 \end{cases} \tag{10}$$

All node difference equations are integrated into the algebraic equation group. The deflection value of each node can be obtained by solving the algebraic equation group using Matlab software.

3. Surface Subsidence Prediction of Tingnan Coal Mine

3.1. Geological and Mining Conditions of Tingnan Coal Mine

The Tingnan Coal Mine is located in the central region of the Binchang Mining Area in Changwu County, Xianyang City, Shaanxi Province, China. The surface is a loess plateau landform and is undulating greatly. The mining area strata are Triassic Jurassic Cretaceous and Quaternary from bottom to top, as shown in Figure 5. The Luohe Formation of Cretaceous is an interbedded stratum of coarse-crystal conglomerate, gritstone, and sandstone with an average thickness of 287.1 m and is the primary aquifer in the mining area. The Yanan Formation of Jurassic is the only coal-bearing stratum in the mining area.

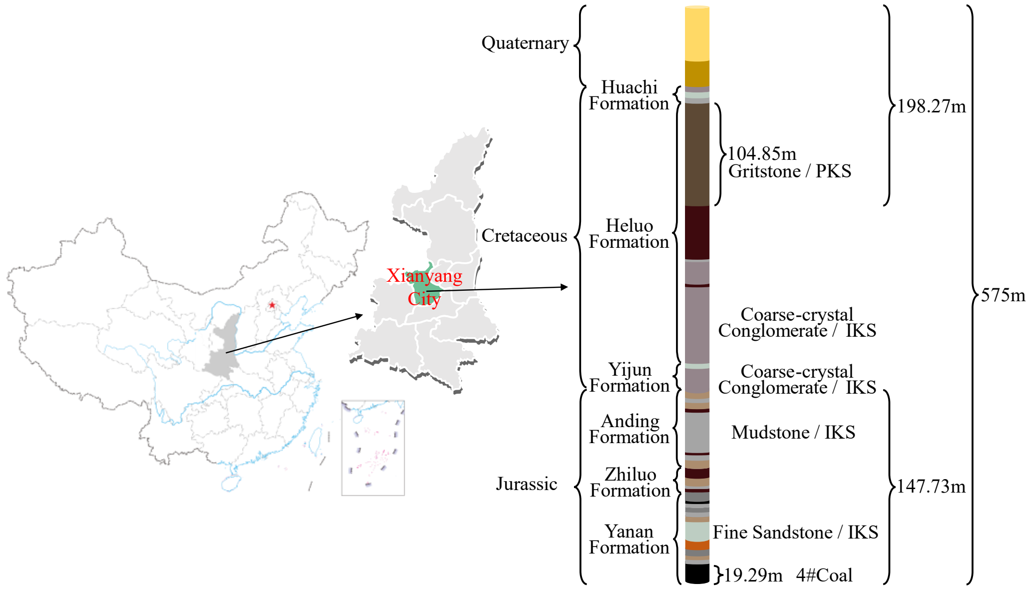

Figure 5. The strata columnar section of ZK9-2 bore-hole [50].

The No. 4 coal seam is mined in the second panel of the Tingnan Coal Mine. The burial depth of the coal seam is 475~653 m. The average burial depth of the coal seam is 575 m. The coal seam is approximately a horizontal distribution. The longwall panel is arranged along the azimuth angle of 0°, as shown in Figure 6. The width of the longwall panel is 200 m, the excavation length of the longwall panel is 2150–2260 m, and the width of the isolated coal pillar is 30 m. The average thickness of the coal seam is 19.0 m and the distance between the coal seam and aquifer of the Heluo Formation is 150–200 m. In order to prevent the fractured water-conducting zone (FWCZ) connecting the aquifer, the mine adopts the height-limiting mining method and the average mining thickness is 6 m. The longwall panel adopts the integrated mechanized backward method with a large mining height. The roof is treated using the full caving method.

During the mining of the 206 longwall panel, the height of the FWCZ was detected through boreholes Y1-1 and Y3. The measured height of the FWCZ is 140.2 m and 148.3 m, respectively [42]. The detection results show that the FWCZ in the Tingnan Coal Mine develop near the lower surface of the Yijun Formation. The gritstone in the Heluo Formation, as the PKS, is located in the continuous deformation zone and appears as elastic deformation.

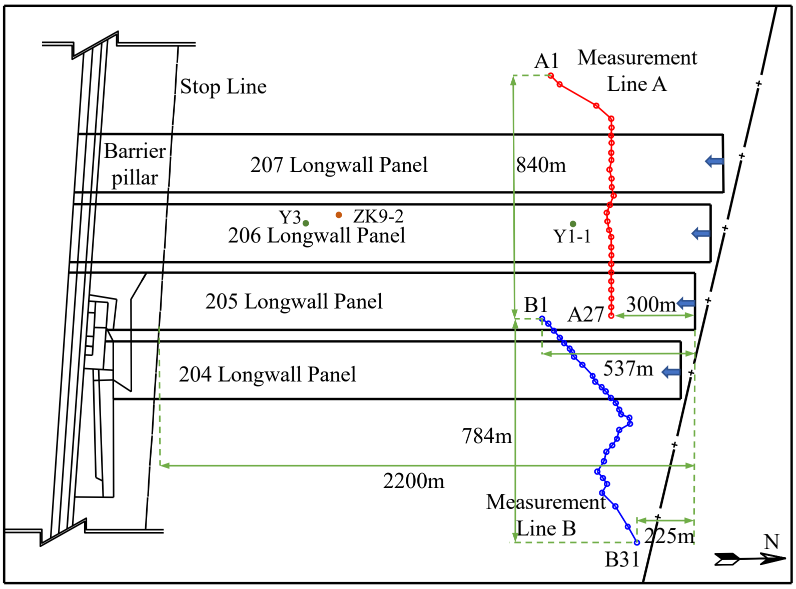

Figure 6. Longwall panel and measurement line [31,42].

3.2. Monitoring of Surface Movement and Deformation

Two monitoring lines of surface movement and deformation are arranged in the second panel. The distance between the A-line and opening of the 205 longwall panel is 300 m. The projection length along the excavation direction is 840 m. 27 measuring points are set in A-line, and the distance between measuring points is 30 m. The distance between the B-line and opening of the 204 longwall panel is 175~487 m. The projection length along the excavation direction is 784 m. 31 measuring points are set in B-line, and the distance between measuring points is 30 m. A-line and B-line are unconventional measurement lines. The available data are the surface subsidence monitoring data of 204, 205, 206 longwall panels. After the surface subsidence of 205 longwall panel is stable, 206 longwall panel begins to be mined. The static GPS, combined with the total station measurement method, is used to observe the surface movement of 205, 206 longwall panels in the early, middle, and stable stages. The monitoring data of the surface movement recession stage are used in the paper.

3.3. Comparative Analysis of Predicted Results and Measured Results

The calculation parameters of the prediction model determined according to the geological and mining conditions of the second panel are shown in Table 1. The average excavation length of the longwall panel is 2200 m. The subsidence curves of the central section are shown in Figure 7. With the increase in the longwall panel length, the area and value of surface subsidence increase. The subsidence curves of the central section in the parallel excavation direction are always in a critical extraction state. When the length of the panel is 1000 m, the subsidence curve of the central section in the parallel panel direction reaches a critical extraction state.

Table 1. The calculation parameters of predicted model [31,42].

E/GPa	h/m	μ	q/MPa	k_g/MPa/m	k_r/MPa/m	α/°	η	H/m
6.3	104.85	0.24	4.23	1.2	5.5	65	0.65	6

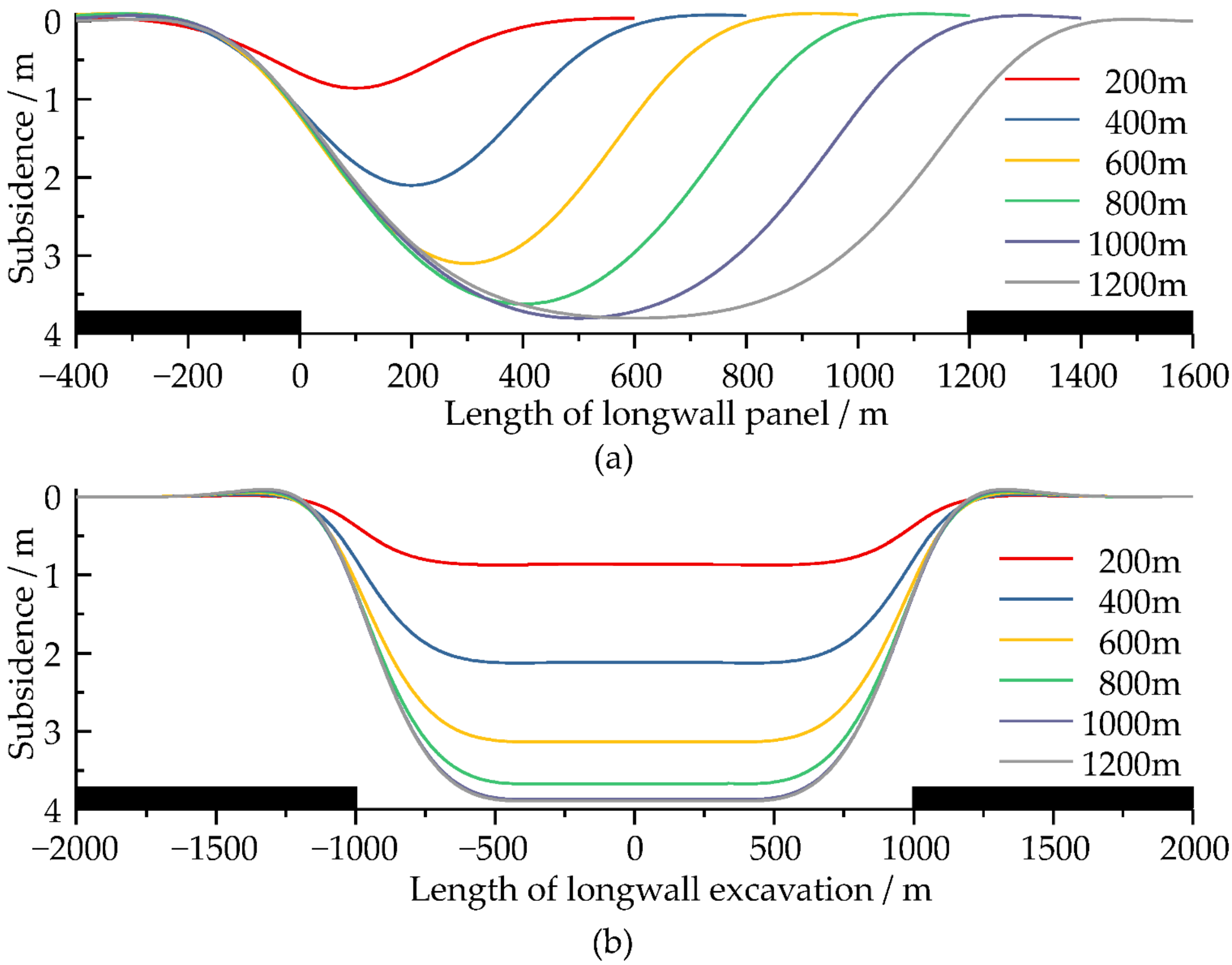

Figure 7. The influence of mining area change on surface subsidence. (**a**) The subsidence curves of the central section in parallel panel direction. (**b**) The subsidence curves of the central section in parallel excavation direction.

Figures 8 and 9, respectively, show the predicted contour maps of surface subsidence after mining in the 204 and 205 longwall panels and in the 204, 205, and 206 longwall panels. Due to the depth of the mining area being less than the average depth of the panel, the predicted results of surface subsidence above the goaf are more than the measured results. At the same time, the surface subsidence is also affected by the isolation coal pillar between the longwall panel. As shown in Figure 8c, the subsidence value of measuring points B3–B5 rebounded due to the influence of isolated coal pillars. Due to the compression deformation of the rock mass, the foundation increases with the increased buried depth around the mining area, hence the predicted results of surface subsidence above the rock mass around the goaf are less than the measured results. It can be seen that with the increase in the mining area, the influence of surface fluctuation and the isolated coal pillar decrease and the matching degree of predicted results increase gradually.

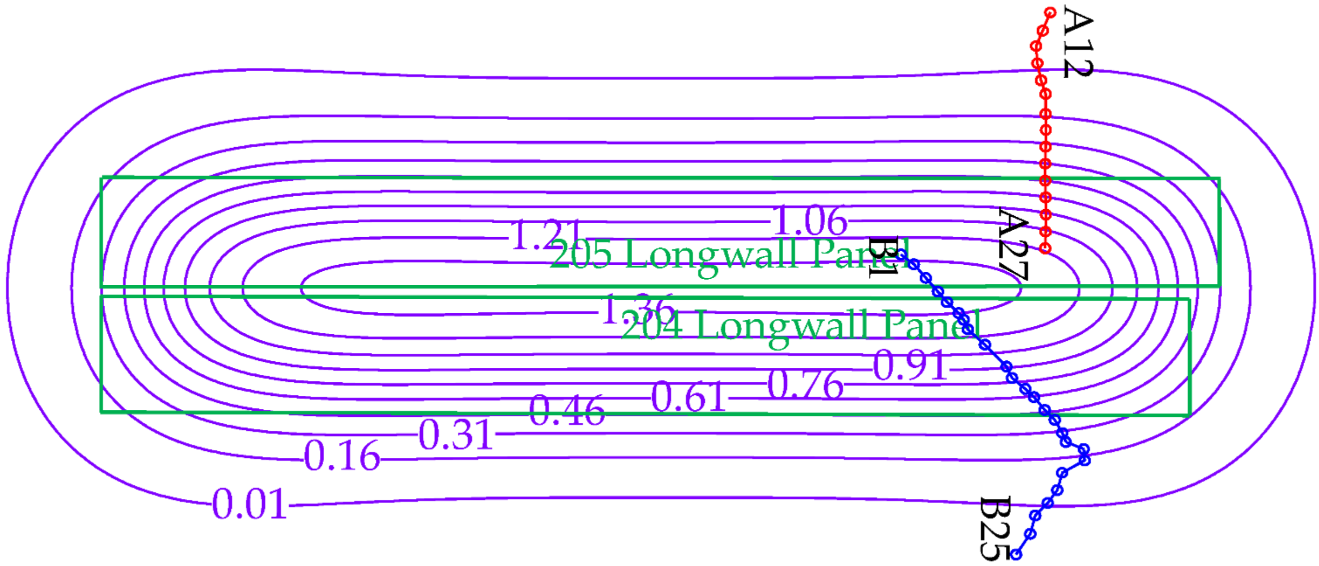

(**a**)

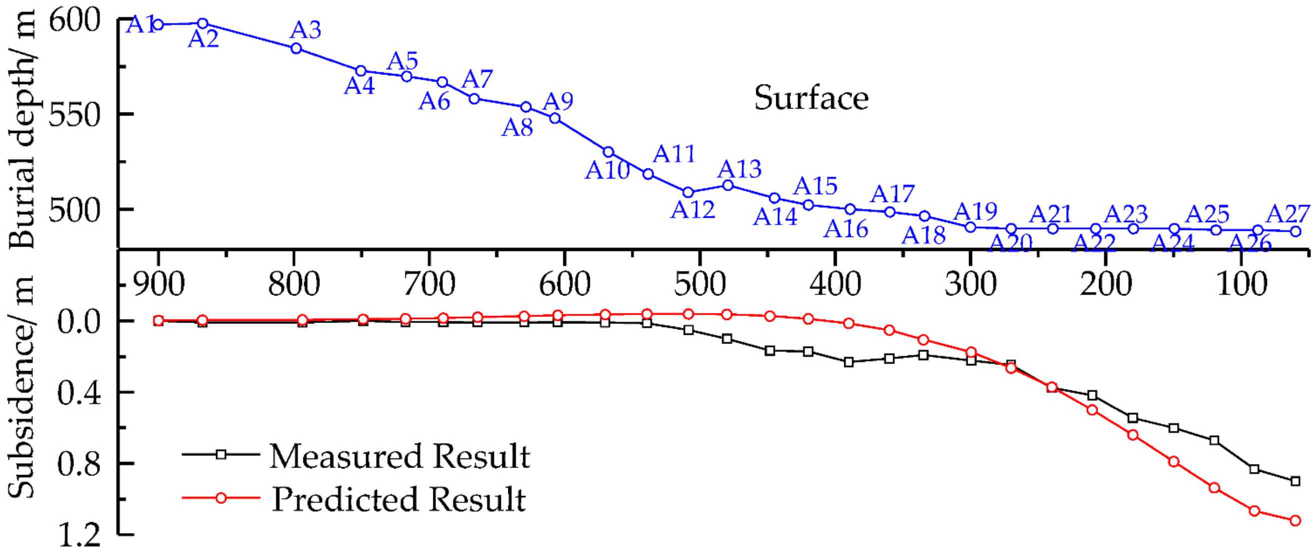

(**b**)

Figure 8. *Cont*.

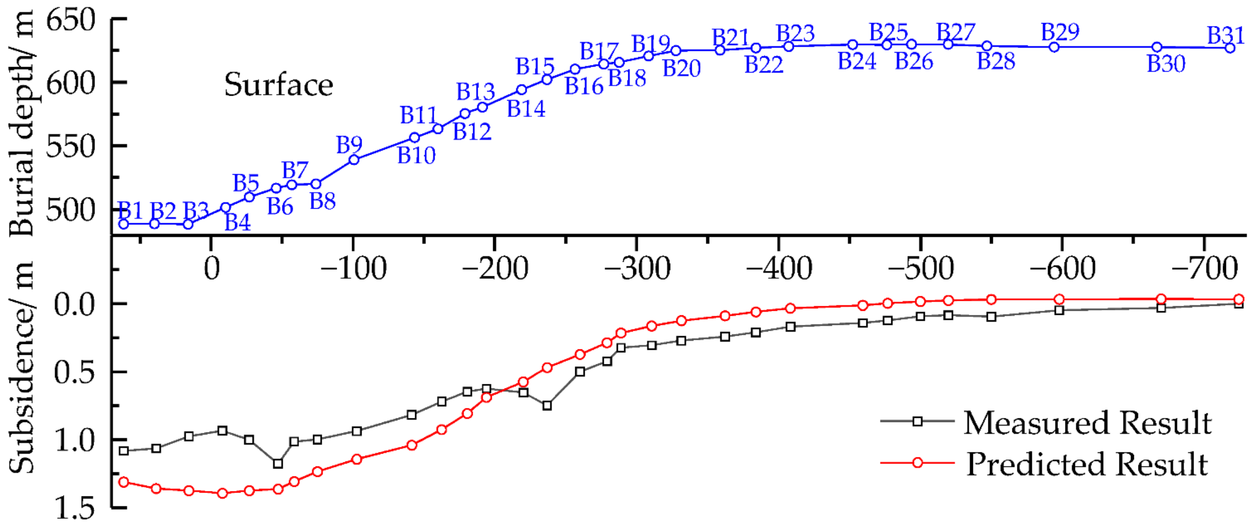

(**c**)

Figure 8. Surface subsidence after mining in longwall panels 204 and 205. (**a**) Subsidence prediction contour line. (**b**) The measured and predicted results of A-line. (**c**) The measured and predicted results of B-line.

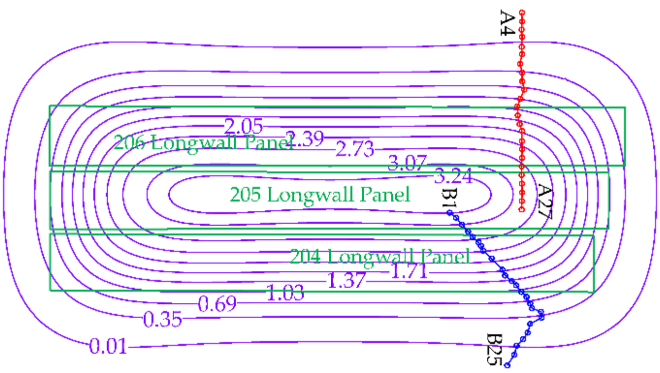

(**a**)

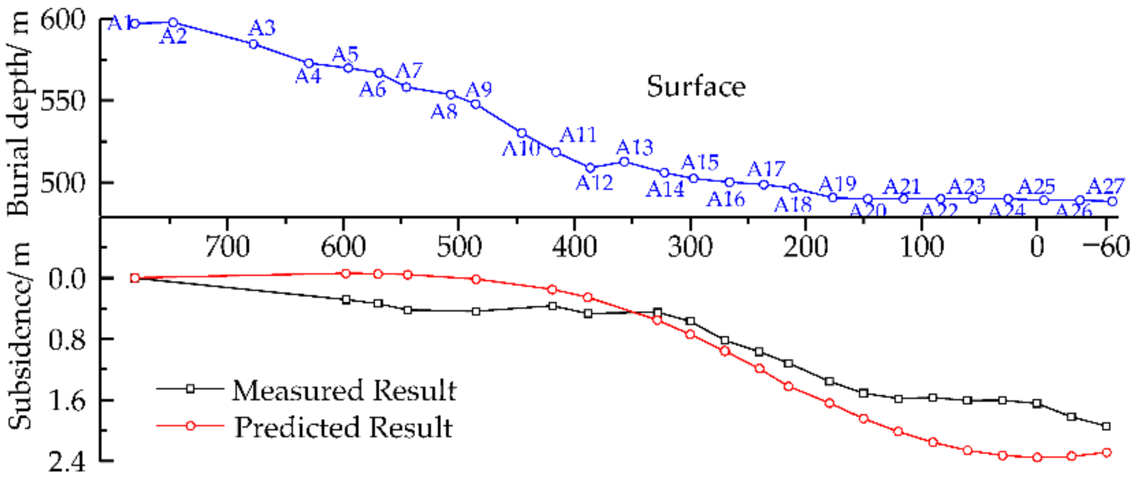

(**b**)

Figure 9. *Cont.*

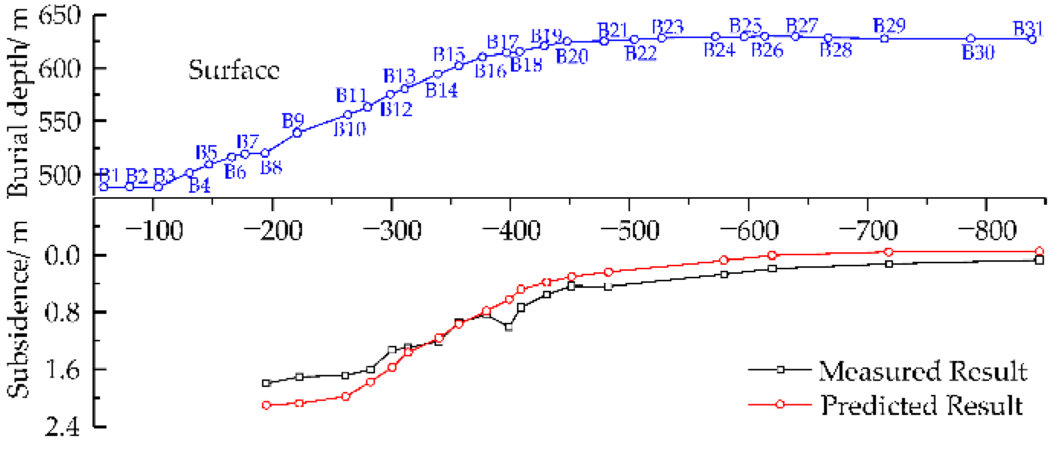

(**c**)

Figure 9. Surface subsidence after mining in longwall panels 204, 205, and 206. (**a**) Subsidence prediction contour line. (**b**) The measured and predicted results of A-line. (**c**) The measured and predicted results of B-line.

4. Discussion

With the geological and mining conditions of the second panel as the research background, the excavation length is 2000 m, and the longwall panel length is 500 m. The prediction model analyzes the influence of load and flexural rigidity of the PKS, goaf foundation modulus, and rock mass foundation modulus on surface subsidence.

Flexural rigidity represents the ability of rock strata to resist deformation. As shown in Figure 10, with the increase in the flexural rigidity of the PKS, the surface subsidence value decreases. The surface subsidence area increases due to the increase in the flexural rigidity of the PKS. The load is affected by the thickness and elastic modulus of the PKS and the thickness and elastic modulus of the controlled rock strata. As shown in Figure 11, the value and area of the surface subsidence increase with the increase in the load of the PKS. The foundation modulus inhibits the surface subsidence. The goaf foundation modulus decreases with the increase in the overburden fracture height and degree of fragmentation. The goaf foundation modulus increases with the increase in distance between the PKS and coal seam. The foundation modulus of the rock mass is affected by each stratum's thickness and elastic modulus between the PKS and coal seam. As shown in Figures 12 and 13, the value and area of the surface subsidence decreased with the foundation modulus of the goaf and rock mass increasing.

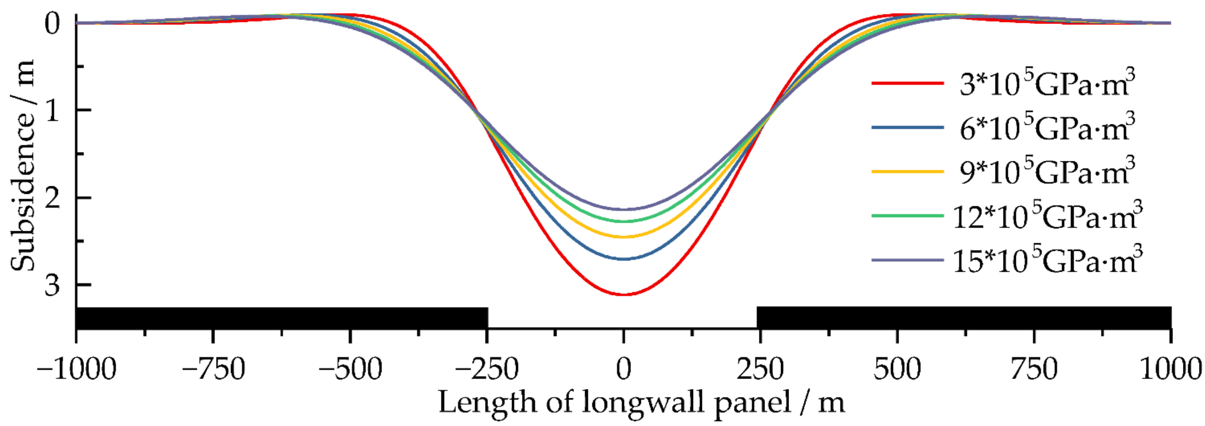

Figure 10. The influence of the flexural rigidity of PKS on surface subsidence.

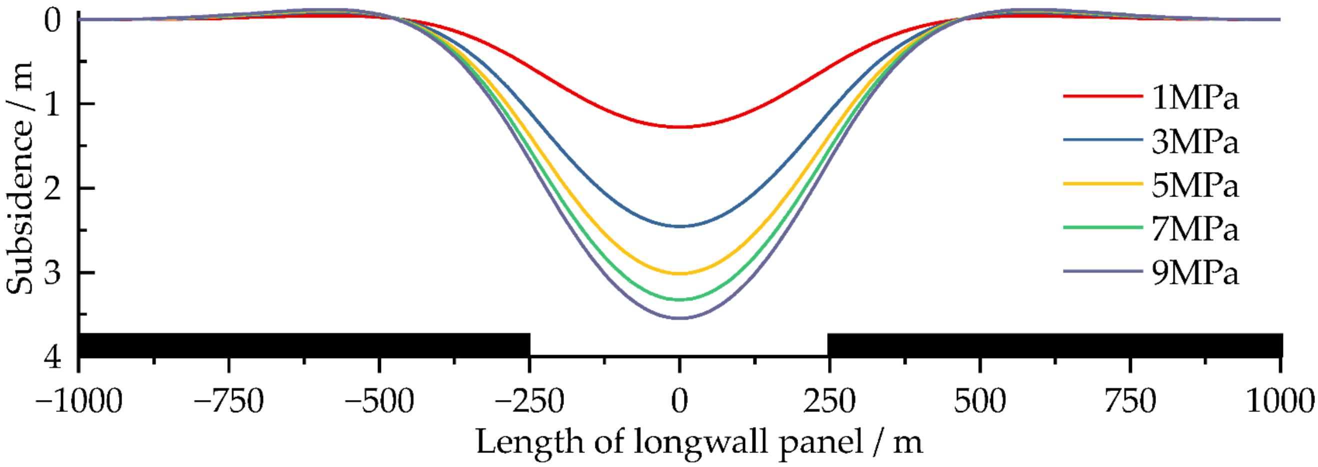

Figure 11. The influence of the load of PKS on surface subsidence.

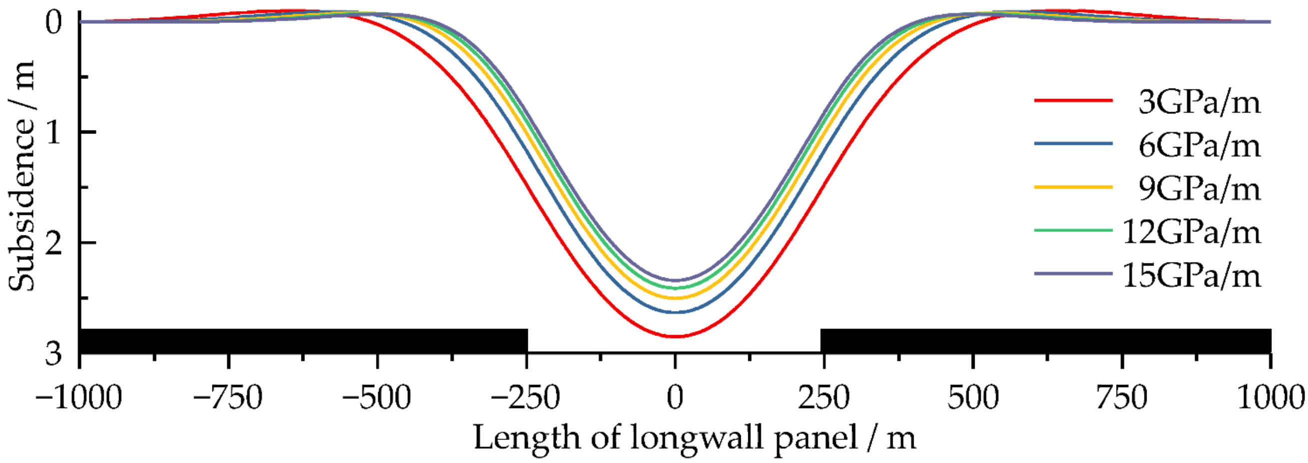

Figure 12. The influence of the foundation modulus of rock mass on surface subsidence.

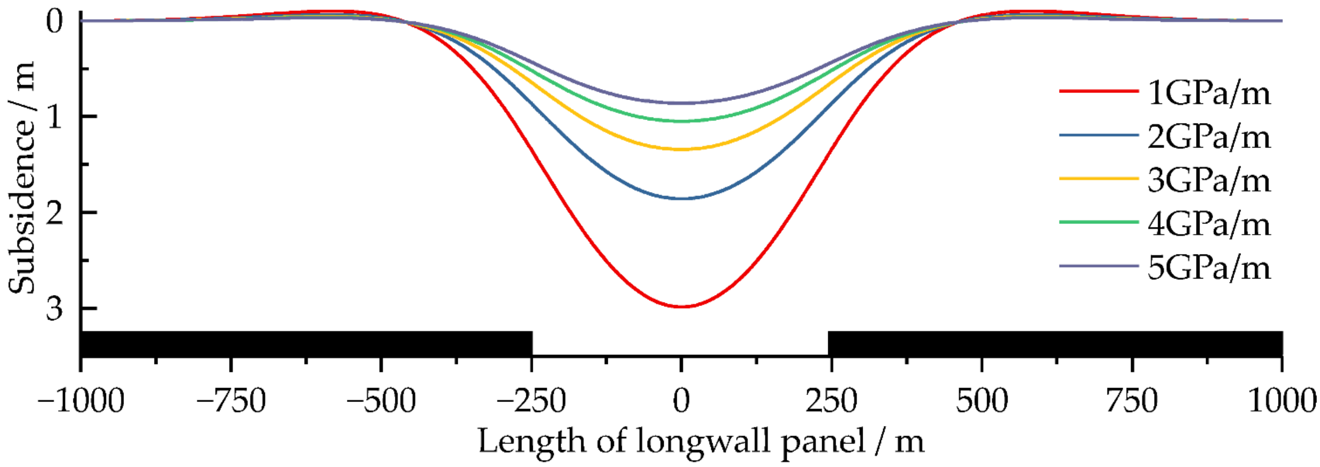

Figure 13. The influence of the foundation modulus of goaf on surface subsidence.

5. Conclusions

This paper analyzes the movement characteristics of mining-induced overburden and establishes a theoretical model of subsidence prediction. The prediction model is verified and discussed by an example. The main conclusions are as follows:

(1) According to the movement characteristics of mining-induced overburden and the key stratum theory, the displacement of the primary key stratum was used to approximately replace the surface subsidence. Based on the thin plate theory supported by the elastic foundation, a full-size mechanical model of the primary key stratum was established and this model predicted the surface subsidence.
(2) The mining subsidence of the second panel of the Tingnan Coal Mine was predicted. Due to the influence of topographic relief and isolated coal pillar, the predicted results of the surface subsidence above the mining area were more than the measured results. The predicted results of the surface subsidence above the rock mass around the goaf were smaller than the measured results. It is foreseeable that the matching degree between the predicted and the measured results will be improved if the constraints of topographic relief and isolated coal pillars are weakened.
(3) With the increase in flexural rigidity of primary key stratum, the goaf foundation modulus, and rock mass foundation modulus, the surface subsidence value decreased. With the increase in the load of the primary key stratum, the surface subsidence value increased. With the increase in the load and flexural rigidity of the primary key stratum, the area of the surface subsidence increased. With the increase in the goaf foundation modulus and rock mass foundation model, the surface subsidence area decreased.

Author Contributions: Writing—original draft, Writing—review and editing, K.W., J.L. and Z.J.; Supervision, K.W. and J.L.; Software, K.W. and J.L.; Conceptualization, K.W. and J.L.; Funding acquisition, Z.J. All authors have read and agreed to the published version of the manuscript.

Funding: This work was supported by the Heilongjiang Natural Science Fund for Excellent Young Scholars Project (YQ2019E033).

Institutional Review Board Statement: Not applicable.

Informed Consent Statement: Not applicable.

Data Availability Statement: The original contributions presented in the study are included in the article, further inquiries can be directed to the corresponding author.

Conflicts of Interest: The authors declare no conflict of interest.

References

1. Sopata, P.; Stoch, T.; Wójcik, A.; Mrocheń, D. Land surface subsidence due to mining-induced tremors in the upper silesian coal basin (poland)-case study. *Remote Sens.* **2017**, *12*, 3923. [CrossRef]
2. Khanal, M.; Hodgkinson, J.H. Subsidence prediction versus observation in Australia: A short comment. *Environ. Impact Assess.* **2020**, *83*, 106479. [CrossRef]
3. Vervoort, A.; Declercq, P.Y. Surface movement above old coal longwalls after mine closure. *Int. J. Min. Sci. Technol.* **2017**, *27*, 481–490. [CrossRef]
4. Sasaoka, T.; Takamoto, H.; Shimada, H.; Oya, J.; Hamanaka, A.; Matsui, K. Surface subsidence due to underground mining operation under weak geological condition in Indonesia. *J. Rock Mech. Geotech. Eng.* **2015**, *7*, 337–344. [CrossRef]
5. Peng, S. Topical areas of research needs in ground control—A state of the art review on coal mine ground control. *Int. J. Min. Sci. Technol.* **2015**, *25*, 1–6. [CrossRef]
6. Lian, X.; Hu, H.; Li, T.; Hu, D. Main geological and mining factors affecting ground cracks induced by underground coal mining in Shanxi Province, China. *Int. J. Coal Sci. Technol.* **2020**, *7*, 362–370. [CrossRef]
7. Vervoort, A. Various phases in surface movements linked to deep coal longwall mining: From start-up till the period after closure. *Int. J. Coal Sci. Technol.* **2021**, *8*, 412–426. [CrossRef]
8. Li, S.; Fan, C.; Luo, M.; Yang, Z.; Lan, T.; Zhang, H. Structure and deformation measurements of shallow overburden during top coal caving longwall mining. *Int. J. Coal Sci. Technol.* **2017**, *27*, 1081–1085. [CrossRef]
9. Ghabraie, B.; Gang, R.; Smith, J.; Holden, L. Application of 3D laser scanner, optical transducers and digital image processing techniques in physical modelling of mining-related strata movement. *Int. J. Rock Mech. Min. Sci.* **2015**, *80*, 219–230. [CrossRef]
10. Ghabraie, B.; Gang, R.; Smith, J.V. Characterising the multi-seam subsidence due to varying mining configuration, insights from physical modelling. *Int. J. Rock Mech. Min. Sci.* **2017**, *93*, 269–279. [CrossRef]
11. Alejano, L.R.; Ramírez-Oyanguren, P.; Taboada, J. FDM predictive methodology for subsidence due to flat and inclined coal seam mining. *Int. J. Rock Mech. Min. Sci.* **1999**, *36*, 475–491. [CrossRef]

12. Sikora, P.; Wesołowski, M. Numerical assessment of the influence of former mining activities and plasticity of rock mass on deformations of terrain surface. *Int. J. Min. Sci. Technol.* **2020**, *31*, 209–214. [CrossRef]
13. Behera, B.; Yadav, A.; Singh, G.S.P.; Sharma, S.K. Numerical modeling study of the geo-mechanical response of strata in longwall operations with particular reference to Indian geo-mining conditions. *Rock Mech. Rock Eng.* **2019**, *53*, 1827–1856. [CrossRef]
14. Jing, L. A review of techniques, advances and outstanding issues in numerical modelling for rock mechanics and rock engineering. *Int. J. Rock Mech. Min. Sci.* **2003**, *40*, 283–353. [CrossRef]
15. Peng, S.; Cheng, J.; Du, F.; Xue, Y. Underground ground control monitoring and interpretation, and numerical modeling, and shield capacity design. *Int. J. Min. Sci. Technol.* **2018**, *29*, 79–85. [CrossRef]
16. Barbato, J.; Hebblewhite, B.; Mitra, R.; Mills, K. Prediction of horizontal movement and strain at the surface due to longwall coal mining. *Int. J. Rock Mech. Min. Sci.* **2016**, *84*, 105–118. [CrossRef]
17. Nicieza, C.G.; Fernández, M.I.Á.; Díaz, A.M.; Vigil, A.E.Á. The new three-dimensional subsidence influence function denoted by *n-k-g*. *Int. J. Min. Sci. Technol.* **2005**, *42*, 372–387. [CrossRef]
18. Sheorey, P.R.; Loui, J.P.; Singh, K.B.; Singh, S.K. Ground subsidence observations and a modified influence function method for complete subsidence prediction. *Int. J. Min. Sci. Technol.* **2000**, *37*, 801–818. [CrossRef]
19. Yuan, Y.; Li, H.; Zhang, H.; Zhang, Y.; Zhang, X. Improving reliability of prediction results of mine surface subsidence of northern Pei County for reusing land resources. *Appl. Sci.* **2020**, *10*, 8385. [CrossRef]
20. Rošer, J.; Potočnik, D.; Vulić, M. Analysis of dynamic surface subsidence at the underground coal mining site in Velenje, Slovenia through modified sigmoidal function. *Minerals* **2018**, *8*, 74. [CrossRef]
21. Eva, J.; Waclawik, P.; Nemcik, J. Assessment of models to predict surface subsidence in the czech part of the upper silesian coal basin-case study. *Acta Geodyn. Et Geomater.* **2020**, *17*, 469–484. [CrossRef]
22. Cai, Y.; Verdel, T.; Deck, O. On the topography influence on subsidence due to horizontal underground mining using the influence function method. *Comput. Geotech.* **2014**, *61*, 328–340. [CrossRef]
23. Xuan, D.; Xu, J.; Zhu, W. Dynamic disaster control under a massive igneous sill by grouting from surface boreholes. *Int. J. Rock Mech. Min. Sci.* **2014**, *71*, 176–187. [CrossRef]
24. Xu, J.; Zhu, W.; Xu, J.; Wu, J.; Li, Y. High-intensity longwall mining-induced ground subsidence in Shendong coalfield, China. *Int. J. Rock Mech. Min. Sci.* **2021**, *141*, 104730. [CrossRef]
25. Ju, J.; Xu, J. Surface stepped subsidence related to top-coal caving longwall mining of extremely thick coal seam under shallow cover. *Int. J. Rock Mech. Min. Sci.* **2015**, *78*, 27–35. [CrossRef]
26. Qian, M.; Xu, J. Behavior of strata movement in coal mining. *J. China Coal Soc.* **2019**, *44*, 973–984. [CrossRef]
27. Dai, H.; Li, P.; Marzhan, N.; Yan, Y.; Yuan, C.; Serik, T.; Guo, J.; Zhakypbek, Y.; Seituly, K. Subsidence control method by inversely-inclined slicing and upward mining for ultra-thick steep seams. *Int. J. Min. Sci. Technol.* **2022**, *32*, 103–112. [CrossRef]
28. Can, E.; Kucu, S.; Mekik, C. Determination of underground mining induced displacements using GPS observations in Zonguldak-Kozlu Hard Coal Basin. *Int. J. Coal Geol.* **2011**, *89*, 62–69. [CrossRef]
29. Fan, H.; Wang, L.; Wen, B.; Du, S. A new model for three-dimensional deformation extraction with single-track InSAR based on mining subsidence characteristics. *Int. J. Appl. Earth Obs. Geoinf.* **2020**, *94*, 102223. [CrossRef]
30. Cui, X.M.; Li, C.Y.; Hu, Q.F.; Miao, X.X. Prediction of surface subsidence due to underground mining based on the zenith angle. *Int. J. Rock Mech. Min. Sci.* **2012**, *60*, 246–252. [CrossRef]
31. He, C.; Xu, J. Subsidence prediction of overburden strata and surface based on the voussoir beam structure theory. *Adv. Civ. Eng.* **2018**, *26*, 61–68. [CrossRef]
32. Guo, Q.; Guo, G.; Lv, X.; Zhang, W.; Lin, Y.; Qin, X. Strata movement and surface subsidence prediction model of dense solid backfilling mining. *Environ. Earth Sci. Vol.* **2016**, *75*, 1426.1–1426.11. [CrossRef]
33. Li, W.X.; Gao, C.Y.; Yin, X.; Li, J.F.; Qi, D.L.; Ren, J.C. A visco-elastic theoretical model for analysis of dynamic ground subsidence due to deep underground mining. *Appl. Math. Model.* **2015**, *39*, 5495–5506. [CrossRef]
34. Han, H.; Xu, J.; Wang, X.; Xie, J.; Xing, Y. Surface Subsidence Prediction Method for Coal Mines with Ultrathick and Hard Stratum. *Adv. Civ. Eng.* **2019**, *2019*, 371438. [CrossRef]
35. Chang, Z.; Wang, J.; Chen, M.; Ao, Z.; Yao, Q. A novel ground surface subsidence prediction model for sub-critical mining in the geological condition of a thick alluvium layer. *Front. Earth Sci.* **2015**, *9*, 330–341. [CrossRef]
36. Ti, Z.Y.; Li, J.Z.; Wang, M.; Wang, K.; Jin, Z.P.; Tai, C.W. Fracture mechanism in overlying strata during longwall mining. *Shock Vib.* **2021**, *2021*, 4764732. [CrossRef]
37. Ti, Z.Y.; Li, J.Z.; Wang, M.; Li, X.; Jin, Z.P.; Tai, C.W.; Wang, K. Fracture Characteristics and Zoning Model of Overburden during Longwall Mining. *Shock Vib.* **2021**, *2021*, 2857750. [CrossRef]
38. Palchik, V. Localization of mining-induced horizontal fractures along rock layer interfaces in overburden: Field measurements and prediction. *Econ. Environ. Geol.* **2005**, *48*, 68–80. [CrossRef]
39. Li, Z.; Xu, J.; Ju, J.; Zhu, W.; Xu, J. The effects of the rotational speed of voussoir beam structures formed by key strata on the ground pressure of stopes. *Int. J. Rock Mech. Min. Sci.* **2018**, *108*, 67–79. [CrossRef]
40. Peng, S.S. *Longwall Mining*, 3rd ed.; CRC Press/Balkema: London, UK, 2019. [CrossRef]
41. Qian, M.; Miao, X.; Xu, J.; Mao, X. *Study of Key Strata Theory in Ground Control*; University of Mining and Technology Press: Xuzhou, China, 2003.

42. Sun, Y.; Zuo, J.; Karakus, M.; Wang, J. Investigation of movement and damage of integral overburden during shallow coal seam mining. *Int. J. Rock Mech. Min. Sci.* **2019**, *117*, 63–75. [CrossRef]
43. Li, D.; Li, Y.; Chen, J.; Masoumi, H. An analytical model for axial performance of rock bolts under constant confining pressure based on continuously yielding criterion. *Tunn. Undergr. Space Technol.* **2021**, *113*, 103955. [CrossRef]
44. Li, D.; Ma, S.; Lane, M.; Chang, P.; Crompton, B.; Hagen, S.A. Laboratory Investigations into the Failure Mechanisms of New Yielding and Inflatable Rockbolts Under Axial and Shearing Loading Conditions. *Rock Mech. Rock Eng.* **2022**, *182*, 1–23. [CrossRef]
45. Xu, Z.L. *Elasticity*; Higher Education Press: Beijing, China, 2006.
46. Zuo, J.; Sun, Y.; Li, Y.; Wang, J.; Wei, X.; Fan, L. Rock strata movement and subsidence based on mdda, an improved discontinuous deformation analysis method in mining engineering. *Arab. J. Geosci.* **2017**, *10*, 395. [CrossRef]
47. Zhu, Z.; Li, D. Stability assessment of long gateroad pillar in ultra-thick coal seam: An extensive field and numerical study. *Geomech. Geophys. Geo-Energy Geo-Resour.* **2022**, *8*, 147. [CrossRef]
48. Zhu, Z.J.; Wu, Y.L.; Han, J. A Prediction Method of Coal Burst Based on Analytic Hierarchy Process and Fuzzy Comprehensive Evaluation. *Front. Earth Sci.* **2009**, *9*, 128–137. [CrossRef]
49. Zhu, Z.J.; Wu, Y.L.; Liang, Z. Mining-Induced Stress and Ground Pressure Behavior Characteristics in Mining a Thick Coal Seam with Hard Roofs. *Front. Earth Sci.* **2022**, *10*, 190–202. [CrossRef]
50. Wang, X.; Xu, J.; Han, H.; Ju, J.; Xing, Y. Stepped development characteristic of water flowing fracture height with variation of mining thickness. *J. China Coal Soc.* **2019**, *44*, 3740–3749. [CrossRef]